Helimagnetism and field-induced phases in random $Gd_{64}Sc_{36}$ single crystals

1999 J. Phys.: Condens. Matter 11 7115

(http://iopscience.iop.org/0953-8984/11/37/309)

J. Phys.: Condens. Matter **11** (1999) 7115–7124. Printed in the UK PII: S0953-8984(99)02842-8

Helimagnetism and field-induced phases in random $Gd_{64}Sc_{36}$ single crystals

M Salgueiro da Silva†, J M Moreira†, M M Pereira de Azevedo†,
J A Mendes†, C S de Abreu†, J B Sousa†, R J Melville‡ and S B Palmer‡
† IFIMUP, Faculdade de Ciências da Universidade do Porto, Rua do Campo Alegre, 687, 4050 Porto, Portugal
‡ Department of Physics, University of Warwick, Coventry CV4 7AL, UK

Received 22 March 1999, in final form 15 July 1999

Abstract. We report magnetization, neutron diffraction and elastic constant measurements of the single-crystal rare earth alloy $Gd_{64}Sc_{36}$ as a function of magnetic field. For an a-axis field the material exhibits transitions from helix to fan to basal plane ferromagnet. At low temperatures the looked-in magnetic structure is very sensitive to the application of small fields (∼5 mT).

1. Introduction

Previous neutron diffraction studies in Gd–Sc crystalline (hcp) alloys [1] show a competition between ferromagnetic order developed in Gd-rich alloys and helical magnetic order developed in Sc-rich alloys. Such band RKKY controlled competition, together with the very low basal plane anisotropy and the random distribution of the magnetic ions, leads to a complex magnetic phase diagram near the critical composition $Gd_{70}Sc_{30}$ (at.%) [2]. In this region the alloy system exhibits a tricritical region where the paramagnetic (P), ferro (F) and basal plane helical (BPH) phases mutually coexist (figure 1).

Here we study the field-induced magnetic phases observed in single crystals with composition $Gd_{64}Sc_{36}$, which from previous zero field neutron diffraction work [1] is a simple helimagnet from the Néel point (T_N) down to the lowest temperatures. As the temperature is lowered, the helimagnetic turn angle (ω) decreases smoothly with temperature until, at 30 K, it locks in to a value close to 25.7° where the spiral turns through 360° in 14 basal planes. Even in this locked-in phase the helical structure contains no ferromagnetic component, as indicated by the lack of magnetic contributions to the 100 neutron reflection.

The temperature dependence (4–300 K) of the electrical resistivity (ρ, $\mathrm{d}\rho/\mathrm{d}T$), thermoelectric power (S, $\mathrm{d}S/\mathrm{d}T$) and the elastic constant $C_{33}(T)$ have been previously reported for $Gd_{64}Sc_{36}$ in zero applied field [3, 4]. In addition to a sharp minimum observed at the Néel temperature for $\mathrm{d}\rho/\mathrm{d}T$, $\mathrm{d}S/\mathrm{d}T$ and $C_{33}(T)$, a weak anomaly was also noticed in $\mathrm{d}\rho/\mathrm{d}T$ near 70 K.

The present work brings new insight into the magnetic phases of $Gd_{64}Sc_{36}$, especially for the field-induced phases, and is based on a comprehensive analysis of magnetization and elastic constant measurements in the presence of a magnetic field. Several single crystal samples cut either along the c- or a- crystallographic directions were used. Our data spans the temperature range 4–300 K, both with isofield and isothermal curves, using applied magnetic fields up to 1 T for the SQUID measurements and 1.7 T for the elastic constants.

0953-8984/99/377115+10$30.00

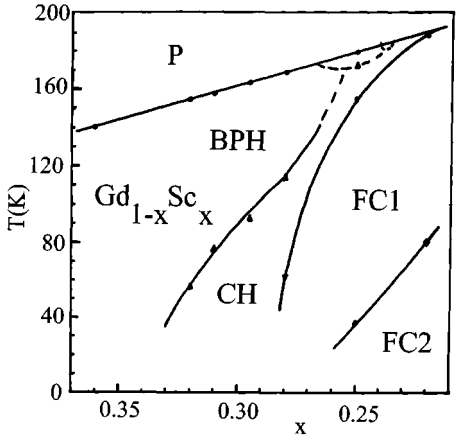

Figure 1. The zero field partial magnetic phase diagram of Gd–Sc random monocrystalline alloys. P—paramagnetic; BHP—basal plane helix; CH—conical helix; FC—ferro canted phase.

The magnetic measurements were made with a commercial Quantum Design SQUID magnetometer with a limiting sensitivity of $\sim 10^{-7}$ emu and point to point repeatability better than 10^{-4}. The elastic constant measurements, made with standard ultrasonic techniques, concentrated on the C_{33} coefficient which is associated with compressional waves propagating along the hexagonal c-axis of the single crystal sample. Since this acoustic mode produces changes in the interatomic spacing along the c-axis it is well known that it couples strongly to the magnetic structure. A measurement of C_{44}, associated with a shear wave propagating down the c-axis, is also included for comparison.

2. Results

2.1. SQUID magnetization measurements

2.1.1. Isofield curves. For these measurements we used a long $Gd_{64}Sc_{36}$ single crystal (6 mm × 1 mm × 1 mm) oriented along the basal plane a-axis, and the magnetic field (H) was applied along this axis to ensure a small demagnetizing factor.

Figure 2 shows the temperature dependence of the isofield ($\mu_0 H = 5$ mT) magnetization, measured in increasing temperature, after cooling the sample from room temperature, either in zero field (ZFC) or under a constant 5 mT field (FC).

The magnetization curve $M(T)$ measured from the zero field cooled state (ZFC curve) is in keeping with the neutron diffraction data [1]. In fact $M(T)$ exhibits only a faint initial increase with temperature which correlates well with the neutron evidence for a lock-in of the helical turn angle for $T \leqslant 30$ K (see figure 5). Above 30 K $M(T)$ decreases gradually with increasing temperature, reflecting the pronounced increase in the helical turn angle (figure 5) which reduces the helix distortion under H (and thus M). The magnetic curve displays an inflection point at $T^* \sim 70$ K, where $\mathrm{d}\rho/\mathrm{d}T$ also exhibits an anomaly [4], followed by a shallow minimum at 100 K and a steep increase towards a sharp peak near the Néel temperature $T_N \sim 140$ K, due to the usual critical fluctuation effects.

The FC magnetization curve is virtually the same as the ZFC curve except at temperatures below $T^* \sim 70$ K, where increasing hysteresis is observed with $M(\mathrm{FC}) > M(\mathrm{ZFC})$, due to the persistence of a small helix distortion under the FC condition. It is clear that the low

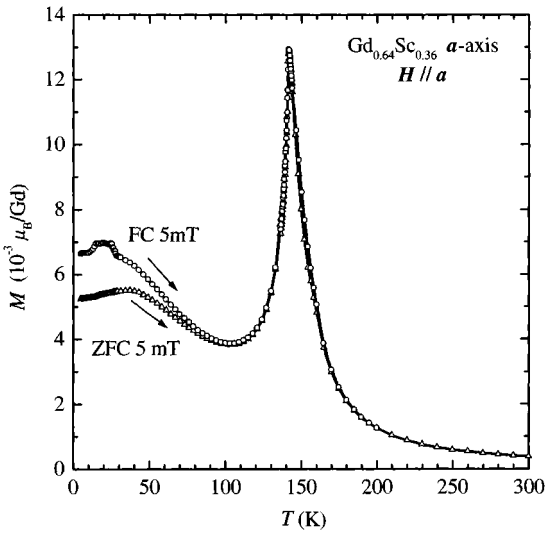

Figure 2. Temperature dependence of the isofield ($\mu_0 H \sim 5$ mT) magnetization (FC—field cooled; ZFC—zero field cooled) for $Gd_{64}Sc_{36}$.

temperature magnetic structure is then modified and in particular one observes in the FC curve two distinct regions: a sudden (steplike) increase appears in the magnetization between 12 and 28 K, followed by a gradual decrease towards the ZFC curve, with a complete merger for temperatures above ∼90 K.

We notice that the anomalous enhancement of the FC magnetization occurs over the restricted temperature range where the zero field helical turn angle approaches a constant value $\omega \sim 26.1^\circ$. We conjecture that the applied field enhances these effects, possibly producing an abrupt lock-in in $\omega(T)$ slightly below 30 K. This could be associated with steplike distortions of the heli-fan structure [5], putting more spins (or component amplitudes) in the direction of the applied field, not excluding spin-slip arrangements [6], so as to give an enhancement of the magnetization.

Such a magnetic-field-stabilized locked structure appears not to persist at low temperatures, and apparently breaks down below ∼12 K, restoring the $M(T)$ curve to its normal trend (as extrapolated from above 30 K). Further neutron studies are required to settle this point.

2.1.2. Isothermal magnetization curves. Figure 3 illustrates the overall behaviour of the basal plane technical magnetization, $M(H)$, both above and below T_N (∼140 K), measured in fields up to 1 T, applied along the *a*-axis. Below T_N and in low fields, where the magnetic moments are helimagnetically ordered with the propagation vector along the *c*-axis [1], the magnetization increases linearly with H. This can be attributed to the distortion of the helimagnetic structure. As shown theoretically [7], and consistent with experiments in simple helimagnets [8], in this field-induced distorted helix structure we still have a periodic rotation (360°) of the basal plane spontaneous magnetization (along the *c*-axis), but the turn angle between consecutive basal planes is not constant, leading to a predominant alignment of the spins along the field direction, thus to a net magnetic moment.

The helix distortion increases with H and then collapses at a critical value H_{c1}, leading to the so-called fan structure, through a first order phase transition, which has been extensively

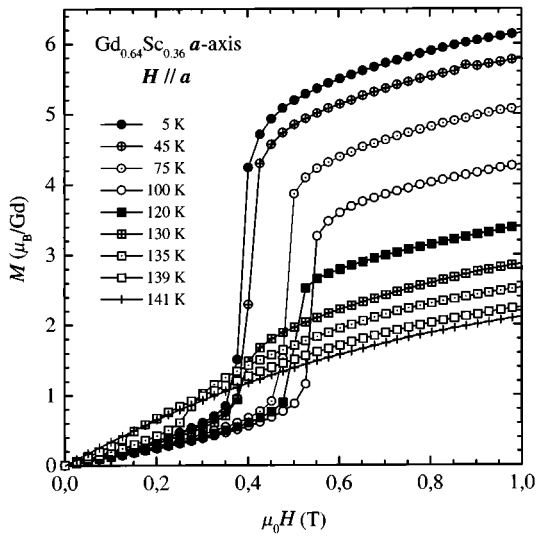

Figure 3. Basal plane technical magnetization, $M(H)$, above and below T_N for $Gd_{64}Sc_{36}$ (*a*-axis field).

modelled [9]. This is clearly seen in our magnetization curves below T_N, which exhibit a sharp discontinuity at a characteristic critical field H_{c1} for each curve. We can extract the temperature dependence of this field over the whole range of temperature below the Néel point (see figure 9).

In the fan phase, the spontaneous magnetization in the different basal planes always has a positive component along the field direction, exhibiting however a characteristic (fanlike) oscillation around the field as we go along the *c*-axis. The corresponding angular oscillation amplitude ($\Delta\Theta$), reminiscent of the helimagnetic turn angle, decreases gradually with the increase of the external field, giving a gradual increase in M, as observed in figure 3. Ultimately, $\Delta\Theta$ reaches zero at a characteristic critical field $H_{c2}(T)$, where the ferromagnetic phase sets in. This occurs through a second order phase transition in our sample, which makes the accurate determination of H_{c2} experimentally difficult.

A magnetic field introduces new effects near the initial helimagnetic ordering temperature. Besides the usual decrease of this critical temperature, the field may also change the initial ordering, from helimagnetic to ferromagnetic-like as shown in figure 4 (isofield curve at 0.4 T). Instead of a sharp peak at T_N, we now observe a knee in the $M(T)$ curve, indicative of the onset of a ferro-like phase. This structure becomes unstable on further decrease of temperature, collapsing into the helimagnetic phase at a characteristic temperature $T \sim 129.5$ K, through a first order phase transition.

2.2. Neutron diffraction results

The neutron experiments were performed under zero magnetic field at the Institute Laue Langevin (Grenoble) using the diffractometer D9. The sample was mounted with the usual orientation for maximum resolution along the *c*-axis [1].

We observe antiferromagnetic satellite reflections at all temperatures below 140 K. In the diffraction pattern, each nuclear reflection hkl is accompanied by a single pair of satellites at $hk\xi$ where $\xi = 1 \pm q$ and q is a displacement in reciprocal lattice units along c^*. The variation

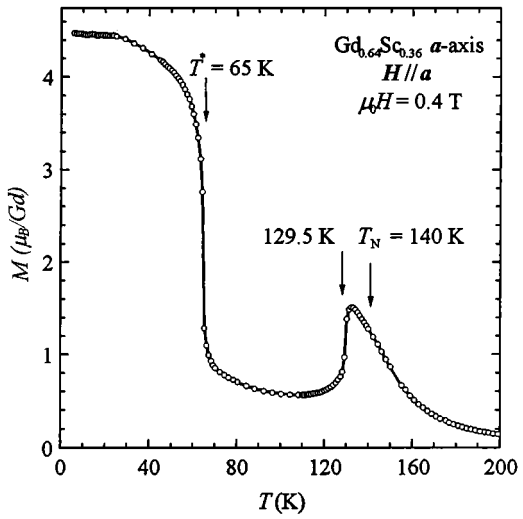

Figure 4. Magnetic moment results, as a function of temperature, for an applied field of 0.4 T along the a-axis. We notice a first order transition at $T^* = 129.5$ K.

of the intensity of satellites centred about different reciprocal lattice points indicates that they arise from a simple helix which propagates along the hexagonal c-axis, and with a turn angle $\omega = \pi q$ between moments in adjacent planes.

The absence of an increase in $(\delta q)^2_{100}$ coincident with the appearance of the satellites means that there is no associated ferromagnetism and the structure is a simple basal plane helix below T_N. As the temperature is lowered the turn angle ω is observed to decrease smoothly from an onset angle of 33.6° per layer (see figure 5). At 30 K, the derivative $\mathrm{d}\omega/\mathrm{d}T$ falls rapidly until the turn angle remains temperature independent at a value $\omega = 26.1 \pm 0.1°$, down to the lowest temperature of 12 K. The locked-in value of ω is incommensurate with the lattice, the nearest commensurate turn angle being 25.7° where the spiral turns through 2π in 14 planes.

Analysis of an isometric plot of the scattered intensity observed in Q-scans through the 101 reflection along the c-axis, as a function of temperature, confirms the behaviour of the turn angle. Also evident is the progressive intensification of the satellites below T_N, consistent with the increase of the spontaneous magnetic moment in the basal plane helix structure. The absence of any magnetic intensity superimposed on the central Bragg peak confirms the absence of a ferromagnetic component in the helical phase of this sample.

2.3. Temperature dependence of the elastic constants

We have measured the C_{33} and C_{44} elastic constants in a $Gd_{64}Sc_{36}$ single crystalline sample. The C_{11} and C_{66} constants were much more difficult to measure due to the much larger thermal contraction and magnetostriction along the c-axis, and are not reported here. The C_{33} and C_{44} results are presented with the elastic constants normalized to their value at room temperature.

The behaviour of C_{33} and C_{44} in zero magnetic field is shown in figures 6 and 7 respectively, with measurements being made while the sample was cooling. We observe an initial dip in C_{33} at the Néel temperature, which is associated with the usual two magnon/one phonon dominant critical coupling, and the sharp recovery is consistent with the basal plane helix structure due to the presence of a single coupling term in the magnetoelastic interaction. By contrast with

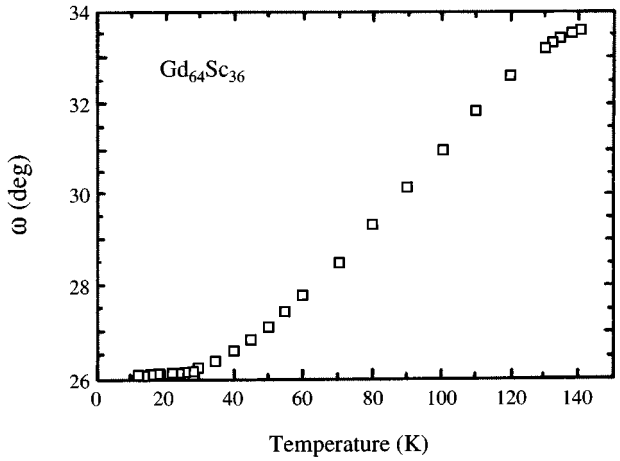

Figure 5. Turn angle (ω) versus temperature (T) for $Gd_{64}Sc_{36}$ as obtained from neutron diffraction work. Notice the lock-in occurring at low temperatures (from [1]).

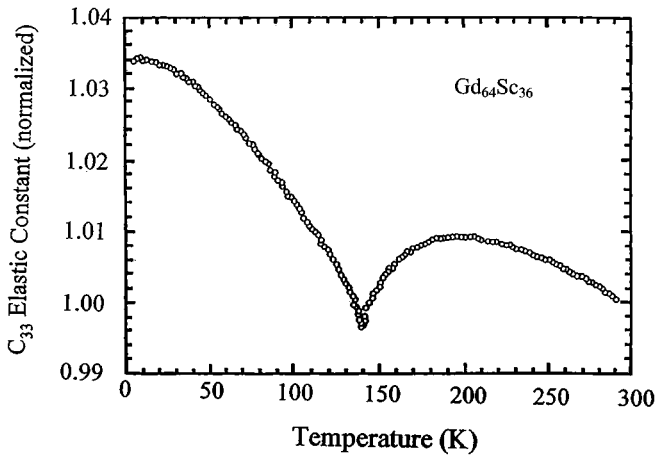

Figure 6. Behaviour of the C_{33} elastic constant as a function of temperature (cooling) for zero applied field.

C_{33}, the C_{44} elastic constant is little affected by the changes occurring in the magnetic structure (figure 7). At T_N, there is a departure from the linear paramagnetic behaviour, towards a slight hardening of C_{44} with decreasing temperature.

2.4. Ultrasonic study of the H–T phase diagram

2.4.1. Isothermal measurements of C_{33} in an applied magnetic field. The magnetic field was applied in the basal plane, using an electromagnet providing a field between 0.007 T (the remanent field) and 1.7 T. The sample used for these particular measurements was a small cube with 4 mm side, and the field was perpendicular to one of the cube's faces. This produces large demagnetization effects, which should be taken into proper account in the analysis of the corresponding $C_{33}(H, T)$ experimental curves.

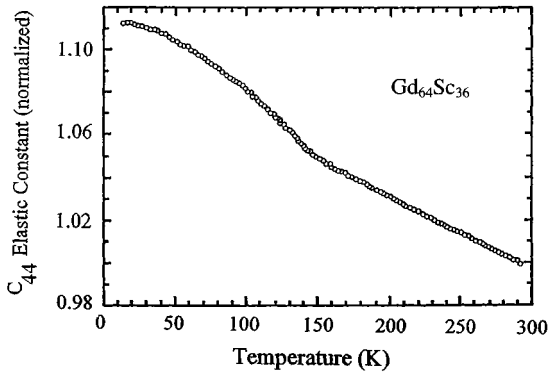

Figure 7. Behaviour of the C_{44} elastic constant as a function of temperature (cooling) for zero applied field.

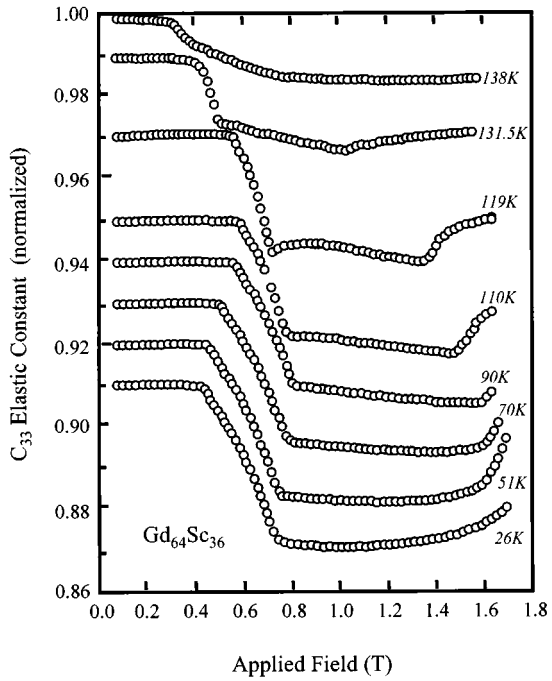

Figure 8. Isothermal measurements of normalized C_{33} elastic constant for a set of temperatures below T_N, as a function of applied basal plane magnetic field.

Figure 8 shows isothermal measurements of (normalized) C_{33} for a variety of temperatures below T_N in an applied magnetic field. Each graph has been displaced along the C_{33} axis for clarity and all exhibit an initial flat (C_{33} constant) region at low fields. This is surprising since the magnetization results (see figure 3) clearly show the effect of a slight distortion of the helix, with the magnetic moments slightly tipped towards the applied field direction. One would then expect this effect to be evident as an initial variation of the magnetoelastic coupling with H, which is not seen in the experimental curves.

However, as H is further increased a critical field H_{c1} is reached where the elastic constant starts to fall sharply. The only exception is the curve at 138 K, where such a decrease is rather smooth and the initial region is not flat. This simply results from the proximity to T_N where the helical structure will be most sensitive to an applied field. From this set of curves we can extract the magnetic phase diagram line $H_{c1}(T)$. The critical field increases from $H_{c1} = 0.42$ T at 26 K, to a maximum $H_{c1} = 0.6$ T at 110 K, and then decreases towards vanishing values at the Néel temperature (see figure 9).

The sharp decrease of C_{33} with H (near H_{c1}) occurs over a field range of about 0.1 T (at 131.5 K) to 0.3 T (at 26 K) representing the transition from a distorted helix to a fan type phase. Ideally one should expect a step discontinuity (as observed in $M(H)$, figure 3), which in the C_{33} measurements, performed in a cubic sample, are smoothed out by large demagnetizing effects.

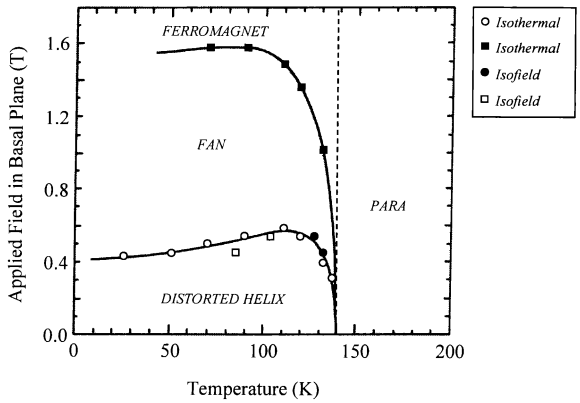

Figure 9. Magnetic phase diagram of $Gd_{64}Sc_{36}$.

In the fan phase C_{33} has a rather small field dependence except at high magnetic fields, when C_{33} starts to harden as the fan structure gets progressively closer to the ferromagnetic phase, and corresponding precursor effects become apparent. The fan–ferromagnetic transition ultimately takes place at a second critical field H_{c2}, which depends on temperature. From the ultrasonic results we obtain, after correction for demagnetization effects: $\mu_0 H_{c2} \sim 0.9$ T at $T \sim 131.5$ K and $\mu_0 H_{c2} \sim 1.2$ T at $T \sim 51$ K. We again notice that demagnetizing effects tend to smear out the transition at H_{c2}. Also, as $T \to T_N$ it is increasingly difficult to identify the fan–ferromagnetic transition and therefore to determine H_{c2} accurately (see figure 8, curve at 138 K).

2.4.2. Isofield C_{33} measurements. The isofield measurements were made in basal plane fields while the temperature was cycled between 4 and 300 K. Figures 10(a), (b) and (c) show results for fields of 0.453, 0.542 and 0.8 T respectively. As the temperature is lowered towards T_N the convex curvature is associated with the two magnon/one phonon magnetoelastic coupling. At ∼140 K, there is a change of slope at 0.453 and 0.542 T and a second downward turn which persists for about 10–15 K (for 0.453 and 0.542 T respectively); this is due to the existence of the fan phase in that temperature range.

The steep hardening of C_{33} which occurs just below ∼130 K is associated with the onset of the distorted helix phase. This distorted helix phase persists down to about 80 K. However,

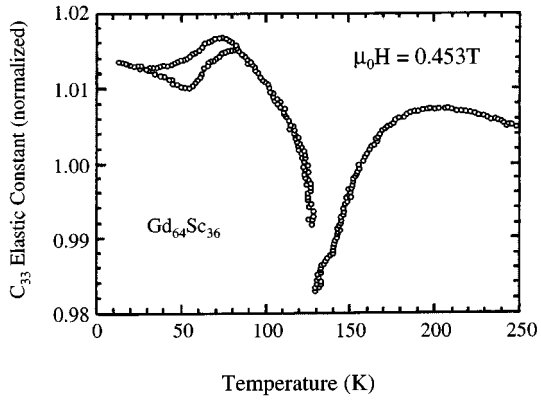

(a)

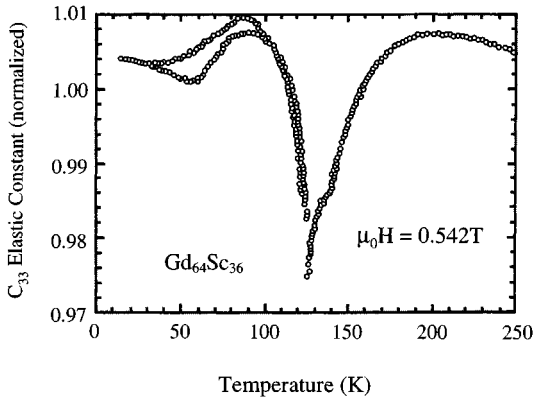

(b)

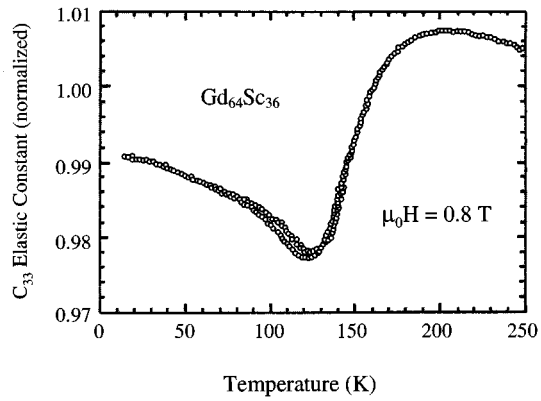

(c)

Figure 10. Isofield C_{33} measurements as a function of temperature, obtained with an applied field of (a) 0.453 T, (b) 0.542 T and (c) 0.8 T.

at lower temperatures the alloy begins to re-enter the fan phase producing again softening of C_{33}. Referring to figure 10(a), obtained with $\mu_0 H = 0.453$ T, we notice that completion of this transition occurs around 30 K where C_{33} reaches a broad minimum. The situation is

further clarified by carrying out measurements on warming from the lowest temperature. We now observe that hysteresis takes place above 30 K, defining a transition region up to ∼80 K, indicative of a mixed phase. Therefore we conclude that the fan phase is fully stabilized below 30 K and no hysteresis is observed. Similar results are obtained with $\mu_0 H = 0.542$ T (figure 10(b)). These results are consistent with the isothermal $M(H)$ measurements (figure 3), and the corresponding transition points have been added to the magnetic phase diagram shown in figure 9.

The behaviour of C_{33} under a large field $H = 0.8$ T is quite different. Just below T_N there is a very slight change in the slope of the curve and a few degrees below we enter a region of slight hysteresis. The phase just below T_N is believed to be the fan phase. The smallness of the hysteresis is consistent with the fact that the fan phase is always dominant, and at 70 K the sample becomes completely ordered in the fan structure once more. The transition temperatures determined from the isofield measurements of C_{33} are also plotted in the phase diagram of figure 9.

3. Conclusions

We have carried out magnetization, neutron diffraction and elastic constant measurements of the single crystalline rare earth alloy $Gd_{64}Sc_{36}$. At zero field the material exhibits a basal plane helical magnetic phase below ∼140 K and the turn angle locks at an incommensurate value below 28 K. At low temperatures the structure is very sensitive to the effect of small applied magnetic fields on cooling. For a magnetic field along the a-axis (basal plane) the material exhibits the usual transitions from helix to fan to basal plane ferromagnet. It is encouraging that all the measurements performed with the three techniques referred above support and complement the phase diagram shown in figure 9. It should be noted that the basic form of this phase diagram is very similar to that found in many of the heavy rare earth elements and alloys and reflects the long range oscillatory nature of the exchange interaction.

Acknowledgments

The authors would like to thank Gary McIntyre for support with the neutron measurements at the Institute Laue Langevin, Grenoble.

References

[1] Melville R J, Bates S, McIntyre G J, Sousa J B and Palmer S B 1988 *Europhys. Lett.* **6** 725
[2] Salgueiro da Silva M, Moreira J M, Mendes J A, Amaral V S, Sousa J B and Palmer S B 1995 *J. Phys.: Condens. Matter* **7** 9853
[3] Melville R J, Palmer S B, McIntyre G J and Sousa J B 1988 *J. Appl. Phys.* **64** 5889
[4] Melville R J, Palmer S B, Sousa J B, Moreira J M, Carvalho C and Pinto R P 1988 *J. Physique Coll.* C **8** 341
[5] Kitano Y and Nagamiya T 1964 *Prog. Theor. Phys.* **31** 1
[6] Cowley R A and Bates S 1988 *J. Phys. C: Solid State Phys.* **21** 4113
[7] Cooper B R and Elliot R J 1963 *Phys. Rev.* **131** 1043
[8] Coqblin B 1977 *The Electronic Structure of Rare-Earth Metals and Alloys* (London: Academic)
[9] Herpin A 1968 *Théorie du Magnétisme* (Paris: Presses Universitaires de France)